CrossMark

TECHNICAL ARTICLE

X-ray powder diffraction study of La_2LiTaO_6

Mark A. Rodriguez,[1,a] James J. M. Griego,[1] Harlan J. Brown-Shaklee,[2] Mia A. Blea-Kirby,[2] John F. Ihlefeld,[2] and Erik D. Spoerke[2]
[1]*Sandia National Laboratories, Materials Characterization and Performance Department, Albuquerque, New Mexico 87185*
[2]*Sandia National Laboratories, Electronic, Optical, and Nanomaterials Department, Albuquerque, New Mexico 87185*

(Received 31 May 2014; accepted 21 October 2014)

The structure of La_2LiTaO_6 has been derived from the powder X-ray powder diffraction (XRD) data. La_2LiTaO_6 is monoclinic with unit-cell parameters $a = 5.621(1)$ Å, $b = 5.776(1)$ Å, $c = 7.954(2)$ Å, $\beta = 90.34(2)°$, space group $P2_1/n$ (14), and $Z = 2$. The structure of La_2LiTaO_6 is an ordered perovskite with alternating Li and Ta octahedra. A new set of powder XRD data (*d*-spacing and intensity listing) has been generated to replace entry 00-039-0897 within the Powder Diffraction File. The newly elucidated structural data for La_2LiTaO_6 shall facilitate quantitative analysis of this impurity phase which is often observed during synthesis of the fast-ion conductor phase $Li_5La_3Ta_2O_{12}$. © *2014 International Centre for Diffraction Data.* [doi:10.1017/S0885715614001183]

Key words: La_2LiTaO_6, X-ray powder diffraction, Rietveld refinement, Li volatility, fast-ion conductor, perovskite

I. INTRODUCTION

Thangadurai *et al.*, (2003) has documented $Li_5La_3Ta_2O_{12}$ as a fast-ion conductor. This compound has a garnet-type structure that displays both a large molar content and a relatively high mobility of Li within the lattice. Therefore, $Li_5La_3Ta_2O_{12}$ and other similar garnet phases are being considered for energy storage applications as separator materials in Li-ion batteries (Thangadurai and Weppner, 2005). The structures of $Li_5La_3Ta_2O_{12}$ and its analog $Li_5La_3Nb_2O_{12}$ have been outlined by Thangadurai *et al.,* (2004) where they note the necessity of employing excess Li during synthesis to account for Li loss because of volatility at high temperatures. Careful control of Li precursor content during synthesis is critical to the formation of these fast Li-ion conductor phases. At times during the processing of $Li_5La_3Ta_2O_{12,}$ an impurity phase of La_2LiTaO_6 may be observed because of the troublesome volatility of the Li species. The presence of La_2LiTaO_6 is a strong indication of Li loss during processing. Hence, determination of the weight fraction of $La_2LiTaO_{6,}$ present in the post-processed $Li_5La_3Ta_2O_{12}$ powders, can aid in the exact determination of the Li excess required in subsequent precursor batching. Powder X-ray Diffraction (PXRD) data for the La_2LiTaO_6 phase has been previously documented in the Powder Diffraction File (PDF) database via entry 00-039-0897 and was initially reported by Hayashi *et al.* (1986) as a *pseudo*-orthorhombic structure. This perovskite lattice demonstrates an ordering of the Li and Ta sites, resulting in doubling of the unit cell in similar fashion to the previously reported La_2LiIrO_6 structure (see Hayashi *et al.* 1980). Various studies on similar ordered perovskite compounds have been reported: Ln_2LiIrO_6 (*Ln* = La, Pr, Nb, Sm, and Eu) by Mugavero *et al.* (2005); La_2LiRuO_6 by Battle *et al.* (2003); La_2LiSbO_6 by Lopez *et al.* (1992). All these studies provide structural details for the documented phases. The existing La_2LiTaO_6 PDF entry 00-039-0897 was based on the information provided from Hayashi *et al.* (1986). This initial report on La_2LiTaO_6 has provided a refined lattice parameters for a monoclinic cell, however, no structural information (i.e. space group, atom positions, occupancies, etc.) were given. Additionally, the absence of an I/I_c value in the PDF entry means, that even semi-quantitative Reference Intensity Ratio analysis cannot be pursued. The absence of this information means detailed quantitative analysis of the La_2LiTaO_6 phase cannot be implemented. Ideally, a full structural elucidation of the La_2LiTaO_6 phase would prove beneficial for such a purpose, thereby allowing quantitative analysis to be performed via Rietveld structure refinement. The purpose of this study was to isolate the La_2LiTaO_6 phase and fully characterize its structure so as to facilitate future means of quantitative XRD.

II. EXPERIMENTAL PROCEDURES

A. Sample synthesis

The La_2LiTaO_6 powder was prepared by solid-state synthesis using Li_2CO_3 (Alfa Aesar, 99.0%), La_2O_3 (Acros, 99.99%), and Ta_2O_5 (HC Starck, 99.0%) precursor powders. The nominal batched composition employed a 1 wt% excess of Li_2CO_3; and precursor powders were ball-milled for 23 h in ethanol (Pharmco-Aaper, 99.5%). The sample powder was calcined at 1000 °C for 12 h (static air atmosphere) using a 5 °C min^{-1} heating rate. After calcination, the sample was ball-milled again to reduce particle size of the La_2LiTaO_6 powder.

B. XRD data collection

A portion of the La_2LiTaO_6 powder was ground in an alumina mortar and pestle and the powder was lightly dusted onto

[a]Author to whom correspondence should be addressed. Electronic mail: marodri@sandia.gov

https://doi.org/10.1017/S0885715614001183 Published online by Cambridge University Press

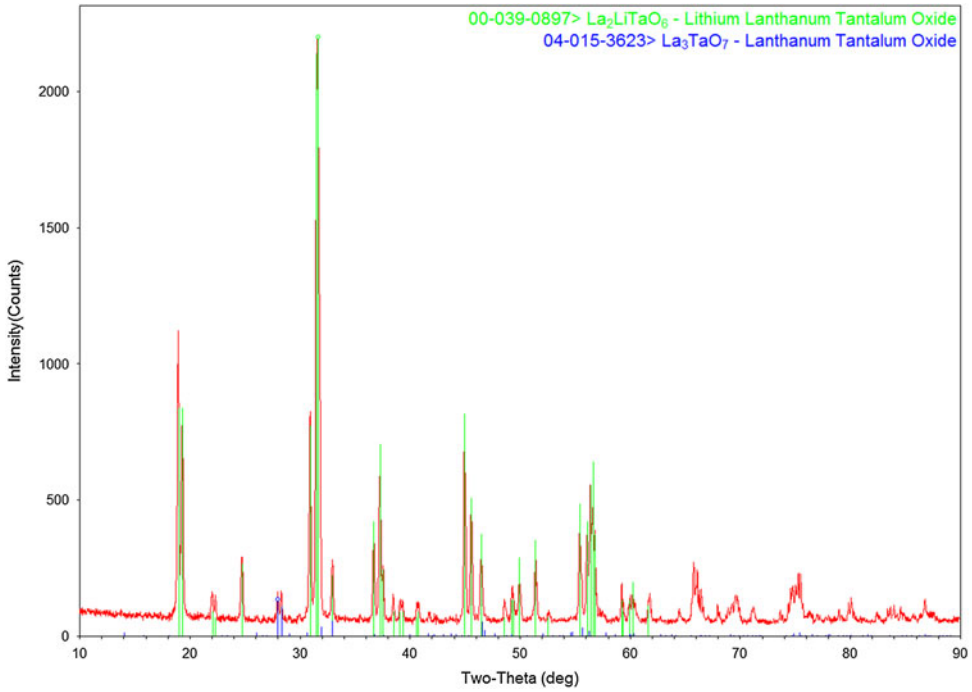


Figure 1. (Color online) XRD pattern for synthesized La_2LiTaO_6 powder is shown as match to the PDF entry 00-039-0897 along with a minor impurity phase of La_3TaO_7.

a greased "zero background" holder (Silicon 510-cut crystal, MTI Corp., Richmond, CA) as outlined by Jenkins and Snyder (1996). This preparation method generated a thin monolayer (~40 to 50 μm) of La_2LiTaO_6 powder for XRD analysis. The relatively high density of La_2LiTaO_6 (~7.2 g cm^{-3}) guaranteed ensured that the monolayer would serve as an infinitely thick specimen for this analysis. A D2 Phaser powder X-ray diffractometer (Bruker AXS, Inc., Madison, WI) equipped with a sealed tube Cu X-ray source (30 kV, 10 mA) and Lynx-Eye 1D energy-discriminating position-sensitive detector was used for data collection. An incident-beam divergence slit (0.6 mm) was employed along with an anti-scatter knife edge (3 mm opening above specimen) to reduce parasitic scatter at the specimen. Powder XRD data were collected over a scan range of 10–90°2θ at a step size of 0.02°2θ and a detector scan-rate of 15°2θ min^{-1}. The equivalent count-time per step in this data collection was ~15 s step^{-1}. Alignment and calibration were checked using a corundum plate (NIST SRM1976) external standard. Diffraction data were collected at room temperature (25 °C).

III. RESULTS AND DISCUSSION

Figure 1 shows the observed XRD powder pattern for La_2LiTaO_6 along with the existing PDF entry 00-039-0897 for La_2LiTaO_6. A small impurity phase of La_3TaO_7 (PDF entry 04-015-3623; Wakeshima *et al.*, 2004) was also observed in the pattern. The presence of La_3TaO_7 suggests the Li volatility in the preparation of the La_2LiTaO_6 phase as well. Fortunately, the La_3TaO_7 impurity phase concentration

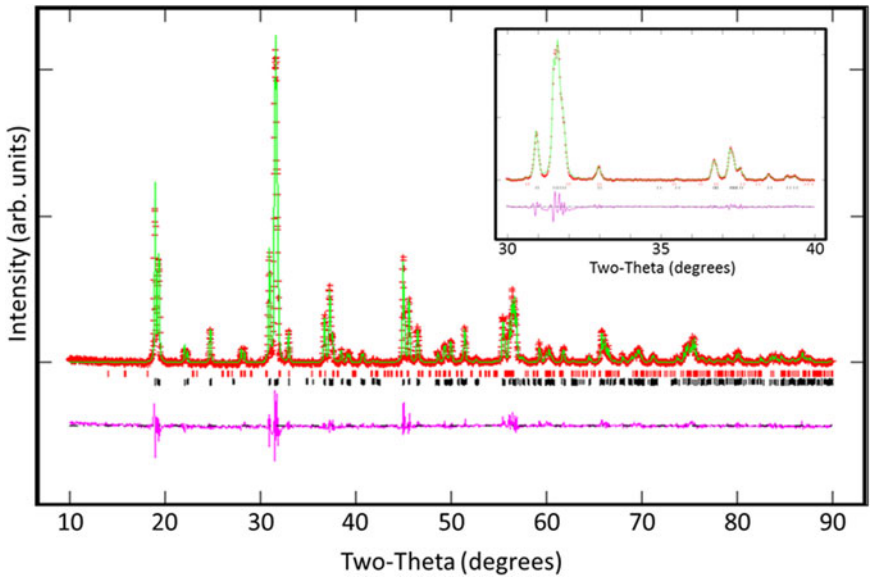


Figure 2. (Color online) Rietveld structure refinement of La_2LiTaO_6 powder as a two-phase refinement including the trace second phase of La_3TaO_7. A zoomed 2θ region is also provided (see inset) to show comparison of fit profiles to that of the raw data. See text for details.

https://doi.org/10.1017/S0885715614001183 Published online by Cambridge University Press

TABLE I. Crystal data and structural refinement for La_2LiTaO_6.

Crystal data
Symmetry: monoclinic
Space group: $P2_1/n$
a (Å) = 5.621(1)
b (Å) = 5.776(1)
c (Å) = 7.954(1)
β (°) = 90.34(2)
Cell Vol (Å^3): 258.25(1)
Z = 2
MW (g mol^{-1}): 1123.39
ρ_x(g cm^{-3}) = 7.22
B_{iso} (Å^2) = 0.3(1)
R_p (%) = 8.70
R_{wp} (%) = 11.18
Reduced χ^2 = 1.260

TABLE II. Refined atomic coordinates for La_2LiTaO_6.

Atom	x	y	z	Occ.
La	0.4900(5)	0.0502(3)	0.2519(3)	1
Li	0	0	0	1
Ta	½	½	0	1
O1	0.209(3)	0.294(3)	0.043(3)	1
O2	0.608(3)	0.473(3)	0.250(2)	1
O3	0.300(3)	0.788(3)	0.046(3)	1

is quite small and will not significantly impact the derivation of structural parameters for the La_2LiTaO_6 phase.

Rietveld structure refinement of the powder XRD data was performed using the EXPGUI version (Toby, 2001) of GSAS (Larson and Von Dreele, 2000). The starting model for the La_2LiTaO_6 in the refinement has employed atom positions for the isostructural compound La_2LiIrO_6 (Mugavero *et al.*, 2005). The structure for La_3TaO_7 was an input from the data supplied by Wakeshima *et al.* (2004). Initial cycles of the two phase refinement converged quickly to low residual error (i.e. $R_p < 10\%$). The background function employed in the refinement was a cosine-Fourier-series (background function option No. 2 in GSAS). Three terms were refined for the background function. The profile function employed for the refinement was the conventional *pseudo-Voigt* function (constant wavelength profile No. 2 in GSAS) where, Lorentzian coefficients for crystallite size and microstrain broadening (Lx and Ly) were refined and the Gaussian variables (U,V,W) were fixed, based on the refinements of the known standard materials (e.g., LaB_6). Specimen shift was also accounted for in the refinement via profile function No. 2 settings, but no asymmetric contributions to the profile were modeled. No evidence of preferred orientation was observed visually from the XRD pattern or during the refinement process (e.g., March–Dollase function refined to unity), so the data were fit without preferred orientation corrections. Figure 2 shows the final fit for the structure refinement showing a satisfactory match with the simulated pattern to that of the raw data. The difference pattern shows minor artifacts associated with small discrepancies in peak shape between the observed peaks and the simulated pattern. A zoomed region (30–40° 2θ) is shown as an inset to Figure 2, better illustrating the fitting of the profiles and residual present in the difference pattern. Crystal data for La_2LiTaO_6 are given in Table I. The refined lattice parameters for La_2LiTaO_6 were very similar to those reported by Hayashi *et al.* (1986) with the exception that the β angle now is reported with a value >90° (i.e. 90.34°). The final residual error (R_p) for the refinement was 8.7% and the reduced χ^2 = 1.26; both these values confirm that the structure refinement is satisfactory and lend validity to the resulting structural parameters obtained. Residual errors (R_p and R_{wp})

TABLE III. PXRD data for La_2LiTaO_6 (reflections with $I_{rel} \leq 0.5\%$ have been removed).

2θ (°)	d (Å)	I_{rel} (%)	Mu	(*hkl*)	2θ (°)	d (Å)	I_{rel} (%)	Mu	(*hkl*)	2θ (°)	d (Å)	I_{rel} (%)	Mu	(*hkl*)
18.972	4.6739	65.7	4	0 1 1	55.394	1.6573	13.7	4	−1 3 2	74.414	1.2739	5.6	4	−3 3 2
19.266	4.6032	25.4	2	−1 0 1	55.481	1.6549	13.6	4	1 3 2	74.640	1.2706	5.7	4	3 3 2
19.376	4.5774	33.9	2	1 0 1	56.108	1.6379	19.6	4	0 2 4	74.779	1.2685	2.9	4	−2 4 1
22.048	4.0283	3.3	4	1 1 0	56.412	1.6298	24.2	4	−3 1 2	74.804	1.2682	2.2	4	0 4 3
22.335	3.9771	2.4	2	0 0 2	56.484	1.6279	10.8	2	−2 0 4	74.854	1.2675	2.8	4	2 4 1
24.711	3.5999	7.6	4	−1 1 1	56.672	1.6229	24.0	4	3 1 2	75.126	1.2635	6.5	4	4 2 0
24.798	3.5876	7.4	4	1 1 1	56.831	1.6187	11.1	2	2 0 4	75.313	1.2609	8.8	4	−1 1 6
30.937	2.8882	44.1	2	0 2 0	57.278	1.6072	2.0	4	−2 2 3	75.538	1.2577	8.9	4	1 1 6
31.518	2.8362	100.0	4	−1 1 2	57.536	1.6006	2.1	4	2 2 3	76.012	1.2510	1.4	4	−2 2 5
31.656	2.8242	99.7	4	1 1 2	59.235	1.5586	4.9	4	−2 3 1	76.161	1.2489	1.2	4	−4 2 1
31.817	2.8103	47.0	2	2 0 0	59.264	1.5580	3.0	4	0 3 3	76.310	1.2469	1.2	4	4 2 1
32.968	2.7147	10.1	4	0 2 1	59.320	1.5566	2.2	4	2 3 1	76.385	1.2458	1.4	4	2 2 5
36.705	2.4465	15.0	4	−1 2 1	59.878	1.5434	2.3	4	−3 2 1	76.968	1.2378	1.2	4	−1 4 3
36.765	2.4426	9.1	4	1 2 1	60.004	1.5405	4.1	4	3 2 1	77.079	1.2363	2.0	4	1 4 3
37.246	2.4122	22.9	4	−2 1 1	60.268	1.5344	2.7	2	−3 0 3	77.820	1.2264	1.6	4	0 3 5
37.286	2.4097	10.9	4	0 1 3	60.296	1.5338	3.7	4	0 1 5	78.595	1.2162	0.6	2	−3 0 5
37.365	2.4048	4.8	4	2 1 1	60.323	1.5331	0.6	2	−1 0 5	79.001	1.2110	2.8	4	4 1 3
37.385	2.4035	3.6	2	−1 0 3	60.531	1.5283	2.1	2	1 0 5	79.148	1.2091	0.6	2	3 0 5
37.563	2.3925	10.6	2	1 0 3	60.642	1.5258	0.9	2	3 0 3	79.872	1.2000	2.1	4	−3 3 3
38.491	2.3370	4.0	4	0 2 2	61.675	1.5027	4.1	4	−1 3 3	79.921	1.1994	2.2	4	−1 3 5
39.106	2.3016	2.9	2	−2 0 2	61.798	1.5000	4.1	4	1 3 3	80.105	1.1971	2.3	4	1 3 5
39.335	2.2887	2.7	2	2 0 2	64.474	1.4441	3.9	2	0 4 0	80.203	1.1959	2.2	4	3 3 3
40.623	2.2191	2.9	4	−1 1 3	65.659	1.4209	4.5	4	0 4 1	82.483	1.1685	3.5	4	0 4 4
40.790	2.2104	3.0	4	1 1 3	65.802	1.4181	13.2	4	−2 2 4	83.468	1.1572	2.8	4	−2 4 3

Continued

https://doi.org/10.1017/S0885715614001183 Published online by Cambridge University Press

TABLE III. Continued

2θ (°)	*d* (Å)	I_{rel} (%)	Mu	(*hkl*)	2θ (°)	d (Å)	I_{rel} (%)	Mu	(*hkl*)	2θ (°)	d (Å)	I_{rel} (%)	Mu	(*hkl*)
41.774	2.1605	0.6	4	−1 2 2	66.119	1.4121	12.8	4	2 2 4	83.687	1.1547	2.8	4	2 4 3
44.970	2.0141	46.1	4	2 2 0	66.487	1.4052	7.0	2	4 0 0	84.035	1.1508	3.6	2	−4 0 4
45.581	1.9886	28.4	2	0 0 4	67.119	1.3935	1.1	4	0 2 5	84.618	1.1444	3.5	2	4 0 4
46.422	1.9545	5.2	4	−2 2 1	67.981	1.3779	2.2	4	−1 4 1	84.718	1.1433	1.2	4	0 5 1
46.455	1.9532	5.8	4	0 2 3	68.020	1.3772	2.2	4	1 4 1	84.740	1.1430	1.0	4	−4 2 3
46.521	1.9505	5.3	4	2 2 1	68.732	1.3646	1.0	4	−2 3 3	85.176	1.1383	1.0	4	4 2 3
48.613	1.8714	5.7	4	0 3 1	68.965	1.3606	3.4	4	2 3 3	85.697	1.1327	1.2	4	−3 4 1
49.284	1.8475	8.2	4	−1 2 3	69.151	1.3574	0.8	4	0 4 2	85.799	1.1316	1.3	4	1 5 0
49.427	1.8425	4.1	4	1 2 3	69.287	1.3550	2.2	4	−3 2 3	85.806	1.1315	1.1	4	3 4 1
49.665	1.8342	2.3	4	−2 1 3	69.339	1.3542	2.8	4	−1 2 5	86.337	1.1259	1.6	4	−2 3 5
49.901	1.8261	2.1	2	−3 0 1	69.532	1.3509	1.0	4	1 2 5	86.482	1.1244	1.9	4	−4 3 1
49.949	1.8244	8.3	4	2 1 3	69.609	1.3496	4.1	4	−2 1 5	86.627	1.1229	0.6	4	4 3 1
50.034	1.8215	0.7	4	1 3 0	69.635	1.3491	2.3	4	3 2 3	86.700	1.1221	1.0	4	2 3 5
50.043	1.8212	2.9	2	3 0 1	69.763	1.3470	4.0	4	−4 1 1	86.858	1.1205	2.6	4	−1 5 1
51.219	1.7821	0.6	4	3 1 0	69.917	1.3444	0.8	4	4 1 1	86.894	1.1201	2.7	4	1 5 1
51.399	1.7763	8.1	4	−1 3 1	69.995	1.3431	1.1	4	2 1 5	87.364	1.1153	1.6	4	3 2 5
51.446	1.7748	7.8	4	1 3 1	71.095	1.3250	2.3	4	−3 3 1	87.400	1.1150	0.9	4	0 1 7
52.516	1.7411	1.1	4	−3 1 1	71.210	1.3231	2.3	4	3 3 1	87.641	1.1125	1.0	2	1 0 7
52.653	1.7369	1.2	4	3 1 1	73.700	1.2844	3.4	4	2 4 0	87.677	1.1121	1.2	2	5 0 1

reported in Table I are "fitted" residual values (i.e. without background subtraction). An overall atomic displacement parameter (B_{iso}) was refined for the structure and yielded a realistic value of 0.3(1) Å^2. Employment of the overall B_{iso} parameter was considerably more stable within the refinement than atomic displacement parameters for individual atoms, which would sometimes refine non-positive definite. The refined quantity of La_3TaO_7 impurity phase was found to be 3.1(2) wt%. Table II lists the atom positions for La, Li, Ta, and O in the La_2LiTaO_6 structure. Li and Ta occupy unique positions, while the La and three oxygen sites have refinable *x*, *y*, and *z* fractional coordinates.

To generate powder XRD data (d's and I's) for La_2LiTaO_6, the refined structural parameters from Tables I and II were entered into the program PowderCell (PowderCell for Windows, Version 2.4) and a list of peak positions and relative intensities was generated within PowderCell. The use of PowderCell to generate the reflection output list was performed as a check to independently verify the pattern and structure. In addition, the PowderCell output was more easily developed into tabular form and so was employed rather than the conventional GSAS output. The resulting peak list is shown in Table III. Peaks with intensities of ≤0.5% have been removed. The XRD data in Table III were generated via PowderCell so as to avoid possible inaccuracies in peak position and intensity that could be caused during profile fitting of the original raw data (as a result of the superimposed presence of the La_3TaO_7 2nd phase). As a check, the newly simulated XRD powder data from Table III (stick pattern) for La_2LiTaO_6 was overlaid onto the raw data pattern (see Figure 3). The new XRD pattern shows excellent agreement with the raw pattern. It is worth pointing out that the original PDF entry 00-039-0897 reported by Hayashi *et al.* (1986) lists an $I_{rel} = 38\%$ for the (011) reflection, whereas

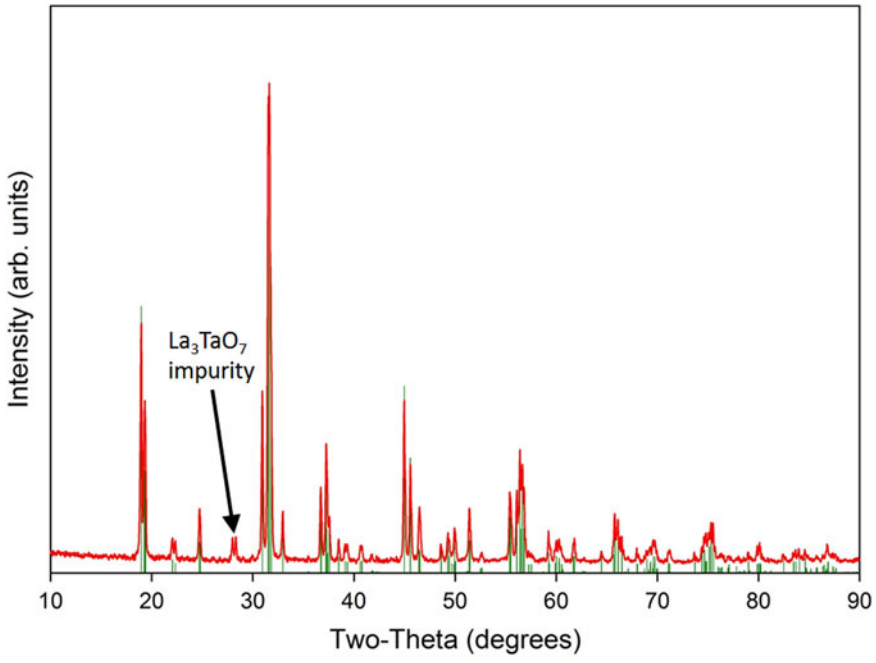


Figure 3. (Color online) New PXRD stick pattern for La_2LiTaO_6 (generated via PowderCell) overlaid onto raw data to verify an acceptable phase identification pattern suitable for the database.

https://doi.org/10.1017/S0885715614001183 Published online by Cambridge University Press

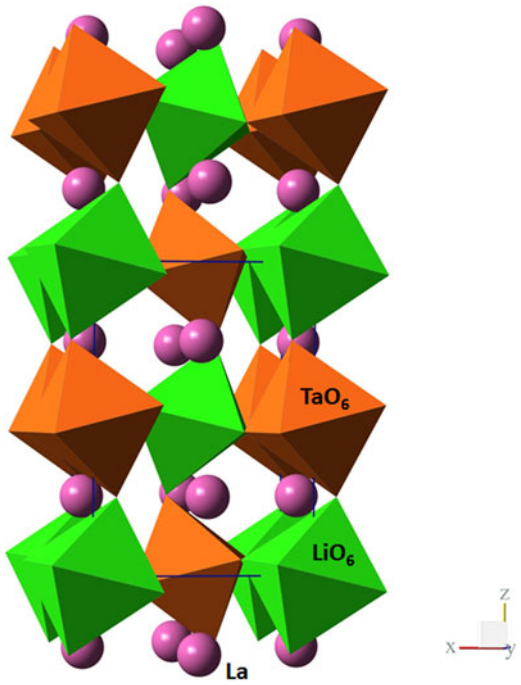


Figure 4. (Color online) Polyhedra visualization of La_2LiTaO_6 structure as viewed down the *b*-axis. Chains of ordered LiO_6 and TaO_6 octahedra are shown propagating along the *c*-axis (vertically) in the image. La atoms are shown as isolated spheres filling the large voids created by the linked octahedra.

results in Table III show a considerably higher value of I_{rel} = 65.7%. Minimal information regarding instrumentation, data collection, and data reduction is given in the Hayashi *et al.*,

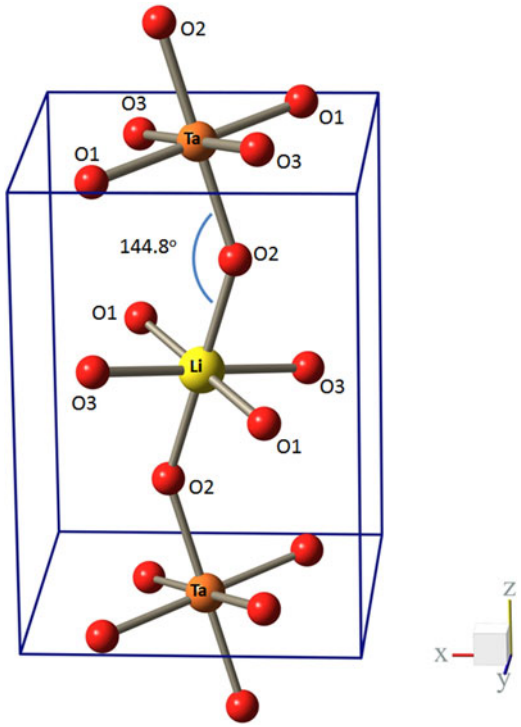


Figure 5. (Color online) Ball and stick visualization of LiO_6 and TaO_6 octahedra showing tilting between linked Li and Ta octahedra as well as relative positioning of the octahedra within the unit cell. See Table IV for Li–O and Ta–O bond lengths. The structure is shown as viewed down the *b*-axis and the *c*-axis propagates vertically. See text for details.

TABLE IV. Selected bond lengths for La_2LiTaO_6.

Bond	Length (Å)
La–O2	2.30(2)
La–O3	2.47(2)
La–O1	2.48(2)
La–O2	2.53(2)
La–O3	2.67(2)
La–O1	2.69(2)
La–O1	2.76(2)
La–O3	2.81(2)
Li–O1×2	2.09(2)
Li–O2×2	2.09(2)
Li–O3×2	2.11(2)
Ta–O1×2	2.05(2)
Ta–O2×2	2.08(2)
Ta–O3×2	2.04(2)

(1986) publication and so it is difficult to assess the origin of this discrepancy. When comparing the balance I_{rel} values from Table III with those reported by Hayashi *et al.* (1986), the trends are more agreeable.

Figure 4 presents the refined structure for La_2LiTaO_6 as a polyhedra model. One can clearly see the ordering behavior of the LiO_6 and TaO_6 octahedra as they stack in the *c*-axis direction. The chains of LiO_6 and TaO_6 show significant octahedral tilting of the apical oxygen (i.e., O2 – see Table II). The La atoms fill the cavities provided by the tilted octahedra. It is the presence of these tilted octahedra, and their respective oxygen locations, that gives rise to significant variability in the La–O bond lengths (as will be discussed later).

Figure 5 better illustrates the ordered LiO_6–TaO_6 chains generated in the structure. This figure shows the apical oxygen (O2) displaying a tilt of 144.8° ± 1.0° for the Li–O2–Ta bond

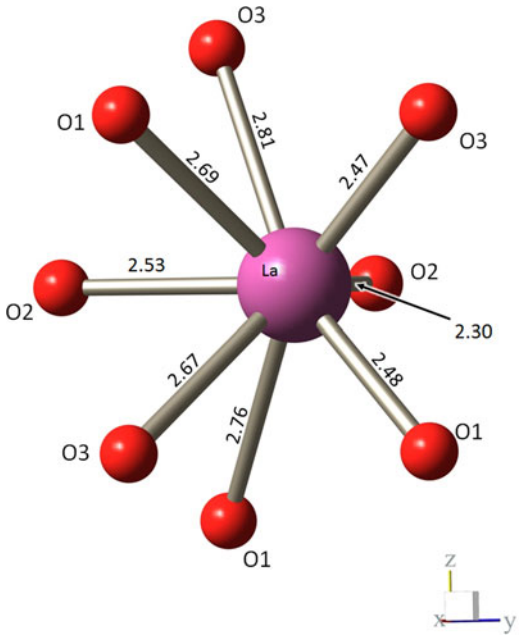


Figure 6. (Color online) Ball and stick visualization of oxygen coordination about the La atom. Numerical values shown on La–O bonds are in Angstroms. See also Table IV for La–O bond lengths. The orientation of this La–O coordination plot has been rotated relative to Figures 4 and 5 and is viewed down the *a*-axis with the *c*-axis propagating vertically.

https://doi.org/10.1017/S0885715614001183 Published online by Cambridge University Press

angle, which is a significant deviation from a linear (180°) arrangement. Although this tilt angle is significant, it is not without precedent, as the isostructural Eu_2LiIrO_6 (see Mugavero *et al.*, 2005) has a comparable tilt angle (144.7°). It is worth pointing out that the tilting of the LiO_6 and TaO_6 octaherdra with respect to one another is quite different along the *c*-axis direction (i.e., Li–O2–Ta bond angle) than the other Li–O–Ta bonding which occurs along the [110] and [−110] directions in the structure. The Li–O–Ta bond angles linking octahedra in these directions, namely Li–O1–Ta (153.4° ± 1.0°) and Li–O3–Ta (151.9° ± 1.1°) display ≈8° anisotropy in the relative orientation of vertex-sharing ochtahedra. Table IV lists the bond lengths for Li–O, Ta–O, and La–O. When considering the Li–O and Ta–O bond lengths, all the Li–O bond values appear similar (between 2.09 and 2.11 Å). The Ta–O bonds are generally shorter (between 2.04 and 2.08). The pervading observation concerning the octahedra is that they are relatively uniform in terms of bond lengths within each respective octahedra (Li or Ta), but there is a significant variance allowed in the tilting of the octahedra when viewed with respect to the neighboring octahedra in the lattice. Figure 6 shows the net effect of the tilt variation on the resulting coordination of the La atom. The La–O bond lengths (in Å) are listed in Figure 6 as well as documented in Table IV. The variation in bond lengths exceeds 0.5 Å as the range of bonds varies from 2.30 to 2.81 Å about the La cation. Similar variations in La–O bond length were observed in the Ln_2LiIrO_6 series (Mugavero *et al.*, 2005) and for La_2LiSbO_6 (Lopez *et al.*, 1992).

IV. CONCLUSION

The La_2LiTaO_6 phase has been isolated and the structure has been refined. The compound displays a monoclinic ordered-perovskite structure. The ordered LiO_6 and TaO_6 octahedra are very similar in terms of metal–oxygen bond uniformity, displaying minimal distortion and uniform bond lengths within each individual LiO_6 or TaO_6 octahedron. However, the linked octahedra display significant Li–O–Ta bond angle tilting, resulting in the distortion of the structure and variable La–O bond lengths. PXRD data have been generated for La_2LiTaO_6 suitable for new entry into the PDF database.

ACKNOWLEDGEMENTS

Material synthesis was supported from the US Department of Energy's Office of Nuclear Energy Fuel Cycle Research and Development Program managed by Dr. Stephen Kung. Sandia National Laboratories is a multiprogram laboratory managed and operated by Sandia Corporation, a wholly owned subsidiary of Lockheed Martin Corporation, for the US Department of Energy's National Nuclear Security Administration under contract DE-AC04-94AL85000.

SUPPLEMENTAL DATA

The supplementary material for this article can be found at http://www.journals.cambridge.org/PDJ.

The Chemical Information File (CIF) for La_2LiTaO_6 is available via the online version.

Battle, P. D., Grey, C. P., Hervieu, M., Martin, C., Moore, C. A., and Paik, Y. (**2003**). "Structural chemistry and magnetic properties of La_2LiRuO_6," J. Solid State Chem. **175**, 20–26.

Hayashi, K., Demazeau, G., Pouchard, M., and Hagenmuller, P. (**1980**). "Preparation and magnetic study of a new iridium (V) perovskite: $LaLi_{0.5}Ir_{0.5}O_3$," Mater. Res. Bull. **15**, 461–467.

Hayashi, K., Noguchi, H., and Fujiwara, S. (**1986**). "New phases in La_2O_3–Li_2O–Ta_2O_3 system," Mater. Res. Bull. **21**, 289–293.

Jenkins, R., and Snyder, R. L. (**1996**). *Introduction to X-Ray Powder Diffractometry* (Wiley, New York), pp. 149–150.

Larson, A. C., and Von Dreele, R. B. (**2000**). *General Structure Analysis System (GSAS)* (Los Alamos National Laboratory Report LAUR 86-748).

Lopez, M. L., Veiga, M. L., Rodriguez-Carvajal, J., Fernandez, F., Jerez, A., and Pico, C. (**1992**). "The Monoclinic Perovskite La_2LiSbO_6. A Rietveld Refinement of Neutron Powder Diffraction Data," Mater. Res. Bull. **27**, 647–654.

Mugavero, S. J., Smith, M. D., and zur Loye, H-C. (**2005**). "The crystal growth and magnetic properties of Ln_2LiIrO_6 (Ln = La, Pr, Nd, Sm, Eu)," J. Solid State Chem. **178**, 200–206.

Thangadurai, V. and Weppner, W. J. F. (**2005**). "$Li_6ALa_2Ta_2O_{12}$ (A = Sr, Ba): novel garnet-like oxides for fast lithium ion conduction," Adv. Funct. Mater. **15**, 107–112.

Thangadurai, V., Kaack, H., and Weppner, W. J. F. (**2003**). "Novel fast lithium ion conduction in garnet-type $Li_5La_3M_2O_{12}$ (M = Nb, Ta)," J. Am. Ceram. Soc. **86**, 437–440.

Thangadurai, V., Adams, S., and Weppner, W. J. F. (**2004**). "Crystal structure revision and identification of Li^+-ion migration pathways in the garnet-like $Li_5La_3M_2O_{12}$ (M = Nb, Ta) oxides," Chem. Mater. **16**, 2998–3006.

Toby, B. H. (**2001**). "EXPGUI, a graphical user interface for GSAS," J. Appl. Crystallogr. **34**, 210–221.

Wakeshima, M., Nishimine, H., and Hinatsu, Y. (**2004**). "Crystal structures and magnetic properties of rare earth tantalates RE_3TaO_7 (RE = Rare Earths)," J. Phys.: Condens. Mater **16**, 4103–4120.

https://doi.org/10.1017/S0885715614001183 Published online by Cambridge University Press